On 3D Numerical Inverse Problems for the Bidomain Model in Electrocardiology

Bedr'Eddine Ainseba, Mostafa Mostafa Bendahmane, Alejandro Lopez

ON 3D NUMERICAL INVERSE PROBLEMS FOR THE BIDOMAIN MODEL IN ELECTROCARDIOLOGY

BEDR'EDDINE AINSEBAA, MOSTAFA BENDAHMANE, AND ALEJANDRO LOPEZ

Abstract. In the inverse problem en electrocardiology, the goal is to recover electrophysiological activity in the heart without measuring directly on its surface (without using catheter interventions). Note that today the inverse computation is frequently used by solving the quasi-static model. This model doesnt take into account the heart dynamic in time and may result in considerable errors in the reconstruction of the solution on the heart. In this paper, a 3D numerical inverse problem constrained by the bidomain equations in electrocardiology is investigated. The state equations consisting in a coupled reaction-diffusion system modelling the propagation of the intracelullar and extracellular electrical potentials, and ionic currents, are extended to further consider the effect of an external bathing medium. Thus, we demonstrate that the novel concept of applying electrophysiological data might be useful to improve noninvasive reconstruction of electrical heart activity. Finally, we present numerical experiments representing the effect of the heart dynamic on the inverse solutions.

1. Introduction

Cardiac related diseases are one of the leading causes of death over the world. Therefore understanding the mechanisms of the electrical activity of the heart could lead to a more accurate diagnosis. A solution would be to measure directly over the heart's surface, but this is highly invasive. Noninvasive means to diagnose disorders of the heart by using noninvasive electrocardiographic imaging (ECGI), this is known as the inverse problem in electrcardiography. The inverse problem in electrocardiography is to reconstruct the electrical cardiac sources from body surface potential measurements (BSPMs), considering the torso as a volume conductor. Solving the inverse problem is beneficial to clinical practice. However, this problem is considered as ill-posed problem. This means that a little variation in the data on the torso will yield unrealistic variations in the reconstructions on the heart. Therefore, it is commonly solved employing regularization techniques (see [12] for more details). To cope the ill-posedness, regularization methods are necessary to arrive at realistic solutions.

The numerical solution of ECG (electrocardiogram) direct and inverse problems has received much attention for many years (and there have been many contributions on this subject). Mostly direct and inverse problems in electrocardiology reduce to a quasistatic Poissons equation with different king of boundary conditions (see for e.g. [31, 13, 30]). For these equations the reconstruction of the solution on the heart is formulated by a linear inverse problem. We know that the analytic solutions of these equations are not difficult to obtain for simple geometries such as cylinders or spheres. Moreover, the difficulties arise when we consider the complex geometries associated with physiological structures (heart, Lungs and torso). Note that the classical inverse problem in electrcardiology doesnt take into account the heart dynamic in time and may result in considerable errors in the reconstruction of the solution on the heart.

It is the purpose of this paper to solve the question of the inverse problem in electrocardiology by using a model consisting of a geometric torso model and a model of the electric activation in the myocardium (the heart) based on the bidomain model. We assume that the medium surrounding the body (the air)

Date: January 15, 2016.

1991 *Mathematics Subject Classification.* 74S05, 65M99, 35K65.

Key words and phrases. Bidomain model, inverse problem, Homogeneous, Non-Homogeneous, electrocardiology, Numerical simulation.

Institut de Mathématiques de Bordeaux UMR CNRS 5251, Université Victor Segalen Bordeaux 2, F-33076 Bordeaux Cedex, France. E-mail: bedreddine.ainseba@u-bordeaux2.fr, mostafa_bendahmane@yahoo.fr.

is nonconductive; thus, the normal derivative of the potential vanishes at the boundary of the insulating medium. Moreover, it is assumed that tissues of the Thorax have a Laplaces equation to govern the potential behaviours according to the theory of the Quasi-static Maxwells equations due to low-frequency response of human tissue.

In our study we reformulate our inverse problem as an optimal control problem where the contraol corresponds to the heart stimulus and thus we can estimate the transmembrane potentials on the heart from the body surface. Note that the regularization in this case is on the heart stimulus and not on the transmembrane potential as in the quasi-static case. Moreover by using the bidomain model, the transmembrane potentials can be used to calculate body surface potentials. Comparing to the quasi-static inverse problem, we show that the dynamic heart model might be useful to improve noninvasive reconstruction of electrical heart activity. Regarding the classical inverse problem, in our method we use an additional step. In this step we compute the transmembrane potential inside the heart from the potential on the heart surface.

This model (introduced by Tung [29]) is one of the most accurate and complete models for the theoretical and numerical study of the electric activity in cardiac tissue.

The bidomain equations result from the principle of conservation of current between the intra- and extracellular domains, followed by a homogenization process (see e.g. [3, 6, 17]) derived from a scaled version of a cellular model on a periodic structure of cardiac tissue. Mathematically, the bidomain model is a coupled system consisting of a scalar, possibly degenerate parabolic PDE coupled with a scalar elliptic PDE for the transmembrane potential and the extracellular potential, respectively. These equations are supplemented by a time-dependent ODE for the so-called gating variable, which is defined at every point of the spatial computational domain. Here, the term "bidomain" reflects that in general, the intra- and extracellular tissues have different longitudinal and transversal (with respect to the fiber) conductivities; if these are equal, then the model is termed *monodomain model*, and the elliptic PDE reduces to an algebraic equation. The degenerate structure of the mathematical formulation of the bidomain model is essentially due to the differences between the intra- and extracellular anisotropy of the cardiac tissue [3, 9].

Before we formulate the inverse problem in mathematical context, we need to introduce the direct problem in electrocardiography. The goal of the direct problem is to compute the body surface potentials from the epicardial potentials. Note that an understanding of the forward problem is a necessary step towards understanding and solving the inverse problem.

In the following section, we formulate both the direct and the inverse problems under some general assumptions about the geometry of the heart-torso system. The remainder of this paper is organized as follows. Section 2 is devoted to the description of our bioelectric model (the bidomain model). Moreover in this section The we state th existence result to direct problem. The discribtion of the inverse problem is given in Section 3. Finally in Section 5, we present the numerical experiments on 3D domains for our dynamic inverse problem. The paper ends with some comments and remarks.

2. The macroscopic bidomain model

The spatial domain of the heart for our models is a bounded open subset $\Omega_H \subset \mathbb{R}^3$ with a piecewise smooth boundary $\partial\Omega_H$. This represents a three-dimensional slice of the cardiac muscle regarded as interpenetrating and superimposed (anisotropic) continuous media, namely the intracellular (i) and extracellular (e) tissues. These tissues are separated from each other (and connected at each point) by the cardiac cellular membrane. The myocardium is surrounded by a volume conductor, Ω_B (the thorax). The quantities of interest are *intracellular*, *extracellular* and the bathing medium electric potentials, $u_{\mathrm{i}} = u_{\mathrm{i}}(x,t)$, $u_{\mathrm{e}} = u_{\mathrm{e}}(x,t)$ at $(x,t) \in \Omega_{H,T} := \Omega_H \times (0,T)$, and $u_{\mathrm{s}} = u_{\mathrm{s}}(x,t)$, at $(x,t) \in \Omega_{B,T} := \Omega_B \times (0,T)$. The myocardium is surrounded by a volume conductor, Ω_B (the thorax). Note that ECG signals monitor the electrical activity of the heart from potential measurements at the torso skin surface $\partial\Omega_T$. The torso volume is commonly modeled as a passive conductor. The differences $v = v(x,t) := u_{\mathrm{i}} - u_{\mathrm{e}}$ and u_{s} are known as the *transmembrane potential* and the depth voltage between the tissue and the bath, respectively. The conductivity of the tissue is represented by scaled tensors $\mathbf{M}_{\mathrm{i}}(x)$ and $\mathbf{M}_{\mathrm{e}}(x)$ given by

$$\mathbf{M}_j(x) = \sigma_j^{\mathrm{t}}\mathbf{I} + (\sigma_j^{\mathrm{l}} - \sigma_j^{\mathrm{t}})\mathbf{a}_l(x)\mathbf{a}_l^{\mathrm{T}}(x),$$

where $\sigma_j^{\mathrm{l}} = \sigma_j^{\mathrm{l}}(x) \in C^1(\mathbb{R}^2)$ and $\sigma_j^{\mathrm{t}} = \sigma_j^{\mathrm{t}}(x) \in C^1(\mathbb{R}^2)$, $j \in \{\mathrm{e}, \mathrm{i}\}$, are the intra- and extracellular conductivities along and transversal to the direction of the fiber (parallel to $\mathbf{a}_l(x)$), respectively. The conductivity tensor of the bathing medium $\mathbf{M}_{\mathrm{s}}$ is assumed to be a diagonal matrice.

For fibers aligned with the axis, $\mathbf{M}_{\mathrm{i}}(x)$ and $\mathbf{M}_{\mathrm{e}}(x)$ are diagonal matrices: $\mathbf{M}_{\mathrm{i}}(x) = \mathrm{diag}(\sigma_{\mathrm{i}}^{\mathrm{l}}, \sigma_{\mathrm{i}}^{\mathrm{t}})$ and $\mathbf{M}_{\mathrm{e}}(x) = \mathrm{diag}(\sigma_{\mathrm{e}}^{\mathrm{l}}, \sigma_{\mathrm{e}}^{\mathrm{t}})$. When the so-called *anisotropy ratios* $\sigma_{\mathrm{i}}^{\mathrm{l}}/\sigma_{\mathrm{i}}^{\mathrm{t}}$ and $\sigma_{\mathrm{e}}^{\mathrm{l}}/\sigma_{\mathrm{e}}^{\mathrm{t}}$ are equal, we are in the case of *equal anisotropy*, but generally the conductivities in the longitudinal direction l are higher than those across the fiber (direction t); such a case is called *strong anisotropy* of electrical conductivity. When the fibers rotate from bottom to top, this type of anisotropy is often referred to as *rotational anisotropy.*

The bidomain model is given by the following coupled reaction-diffusion system [27, 32]:

$$
\begin{aligned}
\beta c_{\mathrm{m}} \partial_t v - \nabla \cdot \big(\mathbf{M}_{\mathrm{i}}(x) \nabla u_{\mathrm{i}}\big) + \beta I_{\mathrm{ion}}(v, w) &= I_i, && (x,t) \in \Omega_{H,T}, \\
\beta c_{\mathrm{m}} \partial_t v + \nabla \cdot \big(\mathbf{M}_{\mathrm{e}}(x) \nabla u_{\mathrm{e}}\big) + \beta I_{\mathrm{ion}}(v, w) &= I_e, && (x,t) \in \Omega_{H,T}, \\
\partial_t w - H(v, w) &= 0, && (x,t) \in \Omega_{H,T}, \\
-\nabla \cdot \big(\mathbf{M}_{\mathrm{s}}(x) \nabla u_{\mathrm{s}}\big) &= 0, && (x,t) \in \Omega_{B,T}.
\end{aligned}
\tag{2.1}
$$

Here, $c_{\mathrm{m}} > 0$ is the *surface capacitance* of the membrane, β is the surface-to-volume ratio, $w(x,t)$ is the *gating* or *recovery variable*, which also takes into account the concentration variables, and I_e, I_i are an external and an internal current stimulus, respectively. The functions $H(v,w)$ and $I_{\mathrm{ion}}(v,w)$ correspond to the fairly simple Mitchell-Schaeffer membrane model [19] for the membrane and ionic currents:

$$
H(v,w) = \frac{w_\infty(v/v_p) - w}{R_{\mathrm{m}} c_{\mathrm{m}} \eta_\infty(v/v_p)}, \quad I_{\mathrm{ion}}(v,w) = \frac{v_p}{R_{\mathrm{m}}} \left(\frac{v}{v_p \eta_2} - \frac{v^2 (1 - v/v_p) w}{v_p^2 \eta_1} \right), \tag{2.2}
$$

where the dimensionless functions $\eta_\infty(s)$ and $w_\infty(s)$ are given by $\eta_\infty(s) = \eta_3 + (\eta_4 - \eta_3)\mathcal{H}(s - \eta_5)$ and $w_\infty(s) = \mathcal{H}(s - \eta_5)$, where $\mathcal{H}$ denotes the Heaviside function, R_{m} is the surface resistivity of the membrane, and v_p and $\eta_1, \dots, \eta_5$ are given parameters. A simpler choice for the membrane kinetics is the widely known FitzHugh-Nagumo model [11, 20], which is often used to avoid computational difficulties arising from a large number of coupling variables. This model is specified by

$$
H(v,w) = av - bw, \quad I_{\mathrm{ion}}(v,w) = -\lambda\big(w - v(1-v)(v-\theta)\big), \tag{2.3}
$$

where a, b, λ, θ are given parameters.

We utilize zero flux boundary conditions for the intracellular potential (the intracellular current does not propagate outside the heart) and we assume there is a perfect transmission between the heart and the torso:

$$
\begin{aligned}
&\big(\mathbf{M}_i(x) \nabla u_i\big) \cdot \mathbf{n} = 0 \text{ on } \Sigma_{H,T} := \partial\Omega_H \times (0,T), \\
&u_e = u_s \text{ and } \big(\mathbf{M}_e(x) \nabla u_e\big) \cdot \mathbf{n} = \big(\mathbf{M}_s(x) \nabla u_s\big) \cdot \mathbf{n} \text{ on } \Sigma_{H,T}, \\
&\big(\mathbf{M}_s(x) \nabla u_s\big) \cdot \mathbf{n}_s = 0 \text{ on } (\partial\Omega_B - \partial\Omega_H) \times (0,T), \\
&u_s = u_c \text{ on } \Sigma_B := (\partial\Omega_B - \partial\Omega_H) \times (0,T)
\end{aligned}
\tag{2.4}
$$

and impose initial conditions (which are degenerate for the transmembrane potential v):

$$
v(0,x) = v_0(x), \quad w(0,x) = w_0(x), \quad x \in \Omega_H. \tag{2.5}
$$

For the solution v of the bidomain model, we require the initial datum v_0 to be compatible with (2.4). Therefore, if we fix both $u_j(0,x)$, $j \in \{\mathrm{e}, \mathrm{i}\}$ as initial data, the problem may become unsolvable, since the time derivative involves only $v = u_{\mathrm{i}} - u_{\mathrm{e}}$ (this is also referred as *degeneracy in time*). Thus, we impose the compatibility condition

$$
\int_{\Omega_H} u_{\mathrm{e}}(x,t)\, dx = 0 \quad \text{for a.e. } t \in (0,T). \tag{2.6}
$$

It is easy to see that the existence of solutions to (4.2), (4.2),, (2.5) requires the compatibility condition

$$
\int_{\Omega_H} I_i(t,x) + I_e(t,x)\, dx = 0 \quad \text{for a.e. } t \in (0,T). \tag{2.7}
$$

Note that in the case that $\mathbf{M}_{\mathrm{i}} \equiv \lambda \mathbf{M}_{\mathrm{e}}$ for some constant $\lambda \in \mathbb{R}$ and , the system (4.2) is equivalent to a scalar parabolic equation for the transmembrane potential v, coupled to an ODE for the gating variable w. This parabolic equation is obtained by multiplying the first equation in (4.2) by $1/(1+\lambda)$, the second by $\lambda/(1+\lambda)$ and adding the resulting equations. The final *monodomain model* can be stated as follows:

$$\begin{aligned} \beta c_{\mathrm{m}} \partial_t v - \nabla \cdot \left(\frac{\mathbf{M}_{\mathrm{i}}}{1+\lambda} \nabla v \right) + \beta I_{\mathrm{ion}}(v, w) = 0, \\ \partial_t w - H(v, w) = 0, \qquad (x,t) \in \Omega_T. \end{aligned} \tag{2.8}$$

This model is, of course, significantly less involved and requires substantially less computational effort than the bidomain model, and even though the assumption of equal anisotropy ratios is very strong and generally unrealistic, the monodomain model is adequate for a qualitative investigation of repolarization sequences and the distribution of patterns of durations of the action potential [8].

We assume that the functions $\mathbf{M}_j$, $j \in \{\mathrm{e}, \mathrm{i}, \mathrm{s}\}$, I_{ion}, g and H are sufficiently smooth so that the following definitions of weak solutions make sense. Furthermore, we assume that $\mathbf{M}_j \in L^\infty(\Omega)$ and $\mathbf{M}_j \boldsymbol{\xi} \cdot \boldsymbol{\xi} \geqslant C_M |\boldsymbol{\xi}|^2$ for a.e. $x \in \Omega$, for all $\boldsymbol{\xi} \in \mathbb{R}^2$, $j \in \{\mathrm{e}, \mathrm{i}, \mathrm{s}\}$, and a constant $C_M > 0$. Observe that in our model one can decompose I_{ion} as

$$I_{\mathrm{ion}}(v, w) =: I_{1,\mathrm{ion}}(v) + I_{2,\mathrm{ion}}(w).$$

Then it is straightforwardly seen that there exists a constant $C_I > 0$ such that (see e.g. [9])

$$\frac{I_{1,\mathrm{ion}}(v_1) - I_{1,\mathrm{ion}}(v_2)}{v_1 - v_2} \geq -C_I, \quad \forall v_1 \neq v_2. \tag{2.9}$$

Additionally, there is a constant $C_I' > 0$ such that

$$0 < \liminf_{|v| \to \infty} \left| \frac{I_{1,\mathrm{ion}}(v)}{v^3} \right| \leq \limsup_{|v| \to \infty} \left| \frac{I_{1,\mathrm{ion}}(v)}{v^3} \right| \leq C_I'. \tag{2.10}$$

We now state the definition of a weak solution for the bidomain model, respectively.

Definition 2.1. *A five-uple* $\mathbf{u} = (v, u_{\mathrm{i}}, u_{\mathrm{e}}, u_{\mathrm{s}}, w)$ *of functions is a* weak solution of the bidomain model (4.2)–(2.5) *if* $v \in L^2(0,T; H^1(\Omega_H)) \cap L^4(\Omega_{H,T})$, $\partial_t v \in L^2(0,T; (H^1(\Omega))^\star) + L^{4/3}(\Omega_{H,T})$, $u_{\mathrm{i}}, u_{\mathrm{e}} \in L^2(0,T; H^1(\Omega))$, $u_{\mathrm{s}} \in L^2(0,T; H^1(\Omega_B))$, $w \in C([0,T], L^2(\Omega))$, (2.6) *is satisfied, and the following identities hold for all test functions* $\varphi_i, \varphi_e \in L^2(0,T; H^1(\Omega_H)) \cap L^4(\Omega_{H,T})$, $\varphi_s \in L^2(0,T; H^1(\Omega_B))$ *and* $\phi \in C([0,T], L^2(\Omega))$*:*

$$\begin{aligned} &\beta c_{\mathrm{m}} \int_0^T \langle \partial_t v, \varphi_i \rangle \, dt + \iint_{\Omega_{H,T}} \Big\{ \mathbf{M}_{\mathrm{i}}(x) \nabla u_{\mathrm{i}} \cdot \nabla \varphi_i + \beta I_{\mathrm{ion}} \varphi_i \Big\} \, dx \, dt = \iint_{\Omega_{H,T}} I_i \varphi_i \, dx \, dt, \\ &\beta c_{\mathrm{m}} \int_0^T \langle \partial_t v, \varphi_i \rangle \, dt + \iint_{\Omega_{H,T}} \Big\{ -\mathbf{M}_{\mathrm{e}}(x) \nabla u_{\mathrm{e}} \cdot \nabla \varphi_e + \beta I_{\mathrm{ion}} \varphi \Big\} \, dx \, dt \\ &\qquad\qquad - \iint_{\Omega_{B,T}} \mathbf{M}_{\mathrm{s}}(x) \nabla u_{\mathrm{s}} \cdot \nabla \varphi_s \, dx \, dt = \iint_{\Omega_{H,T}} I_e \varphi_e \, dx \, dt, \\ &\iint_{\Omega_H} \partial_t w \phi \, dx \, dt = \iint_{\Omega_H} H \phi \, dx \, dt. \end{aligned} \tag{2.11}$$

We have the following result concerning the well-posdness of our model:

Theorem 2.1 (Bidomain model)**.** *If* $v_0 \in L^2(\Omega_H)$, $w_0 \in L^2(\Omega_H)$ *and and* $I_{i,e} \in L^2(\Omega_{H,T})$, *then the bidomain problem* (4.2)-(2.5) *possesses a unique weak solution.*

Proof. First, we introduce the following closed subset of the Banach space:

$$\mathcal{K} = L^2(\Omega_{H,T}).$$

With $\overline{v} \in \mathcal{K}$ fixed, let (v, u_s, w) be the unique solution of the system

$$\begin{cases} \beta c_{\mathrm{m}} \partial_t v - \nabla \cdot \big(\mathbf{M}_{\mathrm{i}}(x) \nabla u_{\mathrm{i}}\big) + \beta I_{\mathrm{ion}}^{\varepsilon}(\overline{v}, w) = I_i, & \text{in } \Omega_{H,T}, \\ \beta c_{\mathrm{m}} \partial_t v + \nabla \cdot \big(\mathbf{M}_{\mathrm{e}}(x) \nabla u_{\mathrm{e}}\big) + \beta I_{\mathrm{ion}}^{\varepsilon}(\overline{v}, w) = I_e, & \text{in } \Omega_{H,T}, \\ \partial_t w - H(v, w) = 0, & \text{in } \Omega_{H,T}, \\ -\nabla \cdot \big(\mathbf{M}_{\mathrm{s}}(x) \nabla u_{\mathrm{s}}\big) = 0, & \text{in } \Omega_{B,T}, \\ \big(\mathbf{M}_i(x) \nabla u_i\big) \cdot \mathbf{n} = 0, & \text{on } \Sigma_{H,T} := \partial\Omega_H \times (0,T), \\ u_e = u_s \text{ and } \big(\mathbf{M}_e(x) \nabla u_e\big) \cdot \mathbf{n} = \big(\mathbf{M}_s(x) \nabla u_s\big) \cdot \mathbf{n}, & \text{on } \Sigma_{H,T}, \\ \big(\mathbf{M}_s(x) \nabla u_s\big) \cdot \mathbf{n}_s = 0, & \text{on } (\partial\Omega_B - \partial\Omega_H) \times (0,T), \\ u_s = u_c, & \text{on } \Sigma_B := (\partial\Omega_B - \partial\Omega_H) \times (0,T), \\ v(0,\cdot) = v_0(\cdot), \quad w(0,\cdot) = w_0(\cdot), & \text{in } \Omega_H, \end{cases} \tag{2.12}$$

where $I_{\mathrm{ion}}^{\varepsilon} = \dfrac{I_{\mathrm{ion}}}{1 + \varepsilon\,|I_{\mathrm{ion}}|}$. Regarding the quasilinear problem (2.12) we have immediatly (see for e.g. [3]): If $v_0 \in L^2(\Omega)$ and $I_{i,e} \in L^2(\Omega_{H,T})$, then there exists a weak solution $v, u_i, u_e \in L^2(0,T; H^1(\Omega_H))$, $\partial_t v \in L^2(0,T; (H^1(\Omega_H))^*)$, $u_s \in L^2(0,T; H^1(\Omega_B))$ and $w \in C(0,T; L^2(\Omega_H))$ to problem (2.12).

In order to prove existence of weak solutions to (2.12), we introduce the map $\Theta : \mathcal{K} \to \mathcal{K}$ satisfying $\Theta(\overline{v}) = v$, where v solves (2.12). By using the Schauder fixed-point theorem, we prove that this map admits a fixed point. First, let us show that Θ is a continuous mapping. Let $(\overline{v}_n)_n$ be a sequence in $\mathcal{K}$ and $\overline{v} \in \mathcal{K}$ be such that $\overline{v}_n \to \overline{v}$ in $L^2(\Omega_H)$ as $n \to \infty$. Define $v_n = \Theta(\overline{v}_n)$, that is, v_n is the solution of (2.12) associated with $\overline{v}_n$. The objective is to show that v_n converges to $\Theta(\overline{v})$ in $L^2(\Omega_H)$.

Multiplying the first, the second, the third and the forth equations in (2.12) by $u_{i,n}$, $-u_{e,n}$, $u_{s,n}$ and w_n, respectively, and integrating over the corresponding domains for $u_{i,n}$, $u_{e,n}$, $u_{s,n}$ and w_n, we arrive at

$$\begin{aligned} \frac{1}{2}\frac{d}{dt} \int_{\Omega_H} (|v_n|^2 + |w_n|^2)\, dx &+ \int_{\Omega_H} \mathbf{M}_{\mathrm{i}}(x) \nabla u_{i,n} \cdot \nabla u_{i,n}\, dx + \int_{\Omega_H} \mathbf{M}_{\mathrm{e}}(x) \nabla u_{e,n} \cdot \nabla u_{e,n}\, dx \\ &+ \int_{\Omega_B} \mathbf{M}_{\mathrm{e}}(x) \nabla u_{e,n} \cdot \nabla u_{e,n}\, dx + \int_{\Omega_H} I_{\mathrm{ion}}^{\varepsilon}(\overline{v}_n, w_n) v_n\, dx - \int_{\Omega_H} H(v_n, w_n) w_n\, dx \\ = \int_{\Omega_H} I_i(x,t) u_{i,n}\, dx &- \int_{\Omega_H} I_e(x,t) u_{e,n}\, dx \\ = \int_{\Omega_H} I_i(x,t) v_n\, dx &- \int_{\Omega_H} (I_e(x,t) - I_i(t,x)) u_{e,n}\, dx. \end{aligned} \tag{2.13}$$

Herein we have used the continuity of the flux and the potentials of the boundary conditions in (2.12). In view of the compatibility condition (2.6), the Poincare inequality and the Young inequalities, it follows from (2.13)

$$\begin{aligned} \frac{1}{2}\frac{d}{dt} \int_{\Omega_H} (|v_n|^2 + |w_n|^2)\, dx + C_1 \int_{\Omega_H} |\nabla u_{i,n}|^2\, dx + C_2 \int_{\Omega_H} |\nabla u_{e,n}|^2\, dx + C_3 \int_{\Omega_B} |\nabla u_{s,n}|^2\, dx \\ \leq C(\varepsilon) + C_4 \int_{\Omega_H} (|v_n|^2 + |w_n|^2)\, dx, \end{aligned} \tag{2.14}$$

for some constants $C(\varepsilon), C_1, C_2, C_3, C_4 > 0$. Therefore an application of Gronwall inequality from (2.14), we get

$$\int_{\Omega_H} |v_n(x,t)|^2\, dx + \int_{\Omega_H} |w_n(x,t)|^2\, dx \leq C_5, \text{ for all } t \in (0,T), \tag{2.15}$$

for some constant $C_5 > 0$. This proves the $L^\infty(0,T; L^2(\Omega))$ bound of v_n and w_n. Moreover using this and (2.14), we arrive at

$$\iint_{\Omega_{H,T}} |\nabla u_{i,n}|^2\, dx\, dt + \iint_{\Omega_{H,T}} |\nabla u_{e,n}|^2\, dx\, dt + \iint_{\Omega_{B,T}} |\nabla u_{s,n}|^2\, dx\, dt \leq C_6, \tag{2.16}$$

for some constant $C_6 > 0$. Observe that there exist $v, u_i, u_e \in L^2(0,T;H^1(\Omega_T))$, $u_s \in L^2(0,T;H^1(\Omega_B))$ and $w \in C(0,T;L^2(\Omega_H))$ such that, up to extracting subsequences if necessary,

$$\begin{aligned}&v_n, u_{i,n}, u_{e,n} \to v, u_i, u_e \text{ in } L^2(0,T;H^1(\Omega_H)) \text{ weakly, } u_{s,n} \to u_s \text{ in } L^2(0,T;H^1(\Omega_B)) \text{ weakly,}\\ &\text{and } w_n \to w \text{ in } L^2(\Omega_T) \text{ strongly,}\end{aligned}$$

and from this the continuity of Θ on $\mathcal{K}$ follows.

It is easy to see that $\Theta(\mathcal{K})$ is bounded in the set

$$\mathcal{W} = \left\{ V \in L^2(0,T;H^1(\Omega_H)) :\ \partial_t V \in L^2(0,T;(H^1(\Omega_H))') \right\}. \tag{2.17}$$

By the results of [26], $\mathcal{W} \hookrightarrow L^2(\Omega_T)$ is compact, thus Θ is compact. Now, by the Schauder fixed point theorem, the operator Θ has a fixed point v such that $\Theta(v) = v$. This implies that there exists a solution $(v_\varepsilon, u_{i,\varepsilon}, u_{e,\varepsilon}, u_{s,\varepsilon}, w_\varepsilon)$ of

$$\begin{aligned}
&\iint_{\Omega_{H,T}} \left\{ \beta c_{\mathrm{m}} \partial_t v_\varepsilon \varphi_i + \mathbf{M}_{\mathrm{i}}(x) \nabla u_{\mathrm{i},\varepsilon} \cdot \nabla \varphi_i + \beta I_{\mathrm{ion}}^\varepsilon \varphi_i \right\} dx\, dt = \iint_{\Omega_{H,T}} I_i \varphi_i \, dx\, dt,\\
&\iint_{\Omega_{H,T}} \left\{ \beta c_{\mathrm{m}} \partial_t v_\varepsilon \varphi_e - \mathbf{M}_{\mathrm{e}}(x) \nabla u_{\mathrm{e},\varepsilon} \cdot \nabla \varphi_e + \beta I_{\mathrm{ion}}^\varepsilon \varphi \right\} dx\, dt\\
&\qquad\qquad\qquad - \iint_{\Omega_{B,T}} \mathbf{M}_{\mathrm{s}}(x) \nabla u_{\mathrm{s},\varepsilon} \cdot \nabla \varphi_s \, dx\, dt = \iint_{\Omega_{H,T}} I_e \varphi_e \, dx\, dt,\\
&\iint_{\Omega_H} w_\varepsilon \partial_t \phi \, dx\, dt = \iint_{\Omega_H} H(v_\varepsilon, w_\varepsilon) \phi \, dx\, dt,
\end{aligned} \tag{2.18}$$

for all test functions $\varphi_i, \varphi_e \in L^\infty(0,T,H^1(\Omega_H))$, $\varphi_s \in L^2(0,T;H^1(\Omega_B))$, and $\phi \in L^2(\Omega_H)$:

Now, substituting $\varphi_i = u_{i,\varepsilon}$, $\varphi_e = -u_{i,\varepsilon}$, $\varphi_s = u_{s,\varepsilon}$ and $\phi = w_\varepsilon$ in (2.18). The result is

$$\begin{aligned}
&\frac{1}{2}\frac{d}{dt} \int_{\Omega_H} (|v_\varepsilon|^2 + |w_\varepsilon|^2)\, dx + \int_{\Omega_H} \mathbf{M}_{\mathrm{i}}(x) \nabla u_{i,\varepsilon} \cdot \nabla u_{i,\varepsilon}\, dx + \int_{\Omega_H} \mathbf{M}_{\mathrm{e}}(x) \nabla u_{e,\varepsilon} \cdot \nabla u_{e,\varepsilon}\, dx\\
&\qquad + \int_{\Omega_B} \mathbf{M}_{\mathrm{e}}(x) \nabla u_{e,\varepsilon} \cdot \nabla u_{e,\varepsilon}\, dx + \int_{\Omega_H} \left(I_{\mathrm{ion}}^\varepsilon v_\varepsilon + C_h \frac{|v_\varepsilon|^2}{1 + \varepsilon\,|I_{\mathrm{ion}}|} \right) dx + \int_{\Omega_H} H(v_\varepsilon, w_\varepsilon) w_\varepsilon \, dx\\
&= \int_{\Omega_H} I_i(x,t) u_{i,\varepsilon}\, dx - \int_{\Omega_H} I_e(x,t) u_{e,\varepsilon}\, dx + C_h \int_{\Omega_H} \frac{|v_\varepsilon|^2}{1 + \varepsilon\,|I_{\mathrm{ion}}|}\, dx\\
&= \int_{\Omega_H} I_i(x,t) v_\varepsilon\, dx - \int_{\Omega_H} (I_e(x,t) - I_i(t,x)) u_{e,\varepsilon}\, dx + C_h \int_{\Omega_H} \frac{|v_\varepsilon|^2}{1 + \varepsilon\,|I_{\mathrm{ion}}|}\, dx.
\end{aligned} \tag{2.19}$$

Using the conditions (2.9) and (2.10) on I_{ion}, the compatibility condition (2.6), Poincare inequality and Young inequalities, we obtain

$$\begin{aligned}
&\frac{1}{2}\frac{d}{dt} \int_{\Omega_H} (|v_\varepsilon|^2 + |w_\varepsilon|^2)\, dx + C_7 \int_{\Omega_H} |\nabla u_{i,\varepsilon}|^2\ dx + C_8 \int_{\Omega_H} |\nabla u_{e,\varepsilon}|^2\ dx + C_9 \int_{\Omega_B} |\nabla u_{s,\varepsilon}|^2\ dx\\
&\qquad \le C_{10} + C_{11} \int_{\Omega_H} (|v_\varepsilon|^2 + |w_\varepsilon|^2)\, dx,
\end{aligned} \tag{2.20}$$

for some constants $C_7, C_8, C_9, C_{10}, C_{11} > 0$ that are independent of ε. Therefore an application of Gronwall inequality we get the $L^\infty(0,T;L^2(\Omega))$ bound of v_ε and w_ε. Using this, (2.20) and the condition on h (...), we get

$$\iint_{\Omega_{H,T}} |I_{\mathrm{ion}}^\varepsilon v_\varepsilon|\ dx\, dt + \iint_{\Omega_{H,T}} |\nabla u_{i,\varepsilon}|^2\ dx + \iint_{\Omega_{H,T}} |\nabla u_{e,\varepsilon}|^2\ dx + \int_{\Omega_{B,T}} |\nabla u_{s,\varepsilon}|^2\ dx\, dt \le C_{12}, \tag{2.21}$$

for some constant $C_{12} > 0$ not depending on ε. Note that the consequence of (2.21) is

$$\iint_{\Omega_{H,T}} |v_\varepsilon|^4\ dx\, dt \le C_{13}, \tag{2.22}$$

for some constant $C_{13} > 0$. In view of (2.20),(2.22) and (2.22), and thanks of the assumption on I_{ion}, we can assume there exist limit functions v, u_i, u_e, u_s, w such that as $\varepsilon \to 0$ the following convergences hold (modulo extraction of subsequences, which we do not bother to relabel):

$$\begin{aligned}
&v_\varepsilon \to v \text{ a.e. in } \Omega_{H,T}, \text{ strongly in } L^2(\Omega_{H,T}), \text{ and weakly in } L^2(0,T;H^1(\Omega_H)),\\
&u_{s,\varepsilon} \to u_s \text{ weakly in } L^2(0,T;H^1(\Omega_B)),\ w_\varepsilon \to w \text{ strongly in } L^2(\Omega_{H,T}),\\
&I^\varepsilon_{\text{ion}}(v_\varepsilon, w_\varepsilon) \to I_{\text{ion}}(v,w) \text{ a.e. in } \Omega_{H,T} \text{ and strongly in } L^1(\Omega_T).
\end{aligned} \tag{2.23}$$

Thanks to all these convergences, it is easy to see that the limit triple (v, u_i, u_e, u_s, w) is a weak solution of (2.8).

□

3. The inverse problem

By an inverse problem we mean the problem of parameter identification, that means we try to determine some of the unknown values of the model parameters according to measurements in a real site and results obtained by simulations. Let V be the vector of parameters to be determined. Essentially, we want to minimize the cost functional:

$$J(I_s) = \iint_{\Sigma_{B,T}} |u_s(t,y,I_s) - u_c(t,y)|^2 \, dy\, dt + \frac{\varepsilon}{2} \iint_{\Omega_{H,T}} |I_s(t,x)|^2 \, dx\, dt, \text{ where } I_s = I_i - I_e. \tag{3.1}$$

3.1. **Minimisation.** In this subsection we prove the existence of optimal solution of (3.1).

Lemma 3.1. *Given $v_0 \in L^2(\Omega)$ and $I_e \in L^2(\Omega_{H,T})$, there exists a solution I_s^* of the optimal control problem (3.1).*

Proof. Let $(I_{s,n})_n$ be a minimizing sequence of (3.1). This means that $J(I_{s,n})$ converges to the infimum of $J(I_s)$ over all feasible (I_s). Next we use (2.23) (where ε and (u_i, u_e, u_s, v, w) are replaced by n and $(u_i^*, u_e^*, u_s^*, v^*, w^*)$) to conclude that

$$u_{s,n} = u_s(t,x,I_{s,n}) \to u_s^*(t,x,I_s) \text{ strongly in } L^2(0,T;H^1(\Omega_B)).$$

Applying the trace theorem (see for e.g. Theorem 6.5 in [18]), we get

$$u_{s,n} = u_s(t,x,I_{s,n}) \to u_s(t,x,I_s) \text{ strongly in } L^2(0,T;L^2(\partial\Omega_B - \partial\Omega_H)).$$

Using this and the weak convergence of $I_{n,s}$ to I_s^* in $L^2(\Omega_{H,T})$, we conclude that the minimization problem (3.1) has a solution I_s^*. □

3.2. **Construction of the Lagrangian.** The Lagrangian related to the optimal control problem is given by

$$\begin{aligned}
\mathcal{L}(\theta) =& \frac{\varepsilon}{2} \iint_{\Omega_{H,T}} |I_i - I_e|^2 \, dx\, dt + \iint_{\Sigma_{B,T}} |u_s(t,y,I_s) - u_c(t,y)|^2 \, dy\, dt \\
&+ \iint_{\Omega_{H,T}} \Big(\beta c_{\text{m}} \partial_t v - \nabla\cdot\, \big(\mathbf{M}_{\text{i}}(x)\nabla u_{\text{i}}\big) + \beta I_{\text{ion}}(v,w) - I_i\Big) p_i \, dx\, dt \\
&- \iint_{\Omega_{H,T}} \Big(\beta c_{\text{m}} \partial_t v + \nabla\cdot\, \big(\mathbf{M}_{\text{e}}(x)\nabla u_{\text{e}}\big) + \beta I_{\text{ion}}(v,w) - I_e\Big) p_e \, dx\, dt \\
&- \int_{\Omega_{B,T}} \nabla\cdot\, \big(\mathbf{M}_{\text{s}}(x)\nabla u_s\big) p_s \, dx\, dt + \iint_{\Omega_{H,T}} \Big(\partial_t w - H(v,w)\Big) q \, dx\, dt + \int_{\Omega_H} \Big(v(x,0) - v_0(x)\Big) z_1 \, dx \\
&+ \iint_{\Sigma_{H,T}} \Big(u_e - u_s\Big) z_2 \, dy\, dt + \iint_{\Sigma_{H,T}} \Big(\mathbf{M}_{\text{e}}(y)\nabla u_{\text{e}} - \mathbf{M}_{\text{s}}(y)\nabla u_{\text{s}}\Big)\cdot\eta\, z_3 \, dy\, dt,
\end{aligned} \tag{3.2}$$

where $\theta = (u_i, u_e, u_s, w, I_i, I_e, I_s, p_i, p_e, p_s, q, z_1, z_2, z_3)$. Observe that from (3.2) we get

$$\left(\frac{\partial \mathcal{L}(u_i, u_e, u_s, w, I_i, I_e, I_s, p_i, p_e, p_s, q, z_1, z_2, z_3)}{\partial I_i}, \delta I_i\right) = ((I_i - I_e) - p_i, \delta I_i),$$

and

$$\left(\frac{\partial \mathcal{L}(u_i, u_e, u_s, w, I_i, I_e, I_s, p_i, p_e, p_s, q, z_1, z_2, z_3)}{\partial I_e}, \delta I_e\right) = (-(I_i - I_e) - p_e, \delta I_e).$$

The first order optimality system is given by the Karusch-Kuhn-Tucker (KKT) conditions which result from equating the partial derivatives of $\mathcal{L}$ with respect to u_i, u_e, u_s and w equal to zero

$$\begin{aligned}
-\beta c_{\mathrm{m}} \partial_t (p_i - p_e) - \nabla \cdot \big(\mathbf{M}_{\mathrm{i}}(x) \nabla p_{\mathrm{i}}\big) + \beta I_{\mathrm{ion}v}(v, w)(p_i - p_e) - H_v(v, w) q = 0, \qquad & (x,t) \in \Omega_{B,T}, \\
-\beta c_{\mathrm{m}} \partial_t (p_i - p_e) + \nabla \cdot \big(\mathbf{M}_{\mathrm{e}}(x) \nabla p_{\mathrm{e}}\big) + \beta I_{\mathrm{ion}v}(v, w)(p_i - p_e) + H_v(v, w) q = 0, \qquad & (x,t) \in \Omega_{B,T}, \\
-\nabla \cdot \big(\mathbf{M}_{\mathrm{s}}(x) \nabla p_{\mathrm{s}}\big) = 0, \qquad & (x,t) \in \Omega_{B,T}, \\
-\partial_t q + \beta I_{\mathrm{ion}w}(v, w)(p_i - p_e) - H_w(v, w) q = 0, \qquad & (x,t) \in \Omega_{H,T}.
\end{aligned} \tag{3.3}$$

Herein $I_{\mathrm{ion}v}$, $I_{\mathrm{ion}w}$, H_v and H_w are the derivative of I_{ion} and H with respect to v, w respectively. We complete the system (3.3) with terminal conditions and boundary conditions:

$$\begin{aligned}
& p_i(\cdot, T) - p_e(\cdot, T) = 0, q(\cdot, T) = 0 \text{ in } \Omega_H \text{ and } p_s(\cdot, T) = 0 \text{ in } \Omega_B, \\
& p_e = p_s \text{ and } \mathbf{M}_{\mathrm{e}}(\cdot) \nabla p_{\mathrm{e}} \cdot \eta = \mathbf{M}_{\mathrm{s}}(\cdot) \nabla p_{\mathrm{s}} \cdot \eta \text{ on } \Sigma_{H,T}, \\
& \mathbf{M}_{\mathrm{s}}(\cdot) \nabla p_{\mathrm{s}} \cdot \eta = 2(u_s - u_e) \text{ on } \Sigma_{T,B}.
\end{aligned} \tag{3.4}$$

4. Numerical approximation for solving the inverse bidomain model

In this section, we present the finite element method for approximation of the inverse bidomain model...

4.1. **A finite element method.** In our discretization for simplicity instead to use the strong coupling boundary conditions (4.1), we utilize the following the following weak coupling boundary conditions: (we assume there is a weak transmission between the heart and the torso):

$$\begin{aligned}
& \big(\mathbf{M}_i(x) \nabla u_i\big) \cdot \mathbf{n} = 0 \text{ on } \Sigma_{H,T} := \partial\Omega_H \times (0, T), \\
& u_e = u_s \text{ and } \big(\mathbf{M}_e(x) \nabla u_e\big) \cdot \mathbf{n} = \big(\mathbf{M}_s(x) \nabla u_s\big) \cdot \mathbf{n} = 0 \text{ on } \Sigma_{H,T}, \\
& \big(\mathbf{M}_s(x) \nabla u_s\big) \cdot \mathbf{n}_s = 0 \text{ on } (\partial\Omega_B - \partial\Omega_H) \times (0, T), \\
& u_s = u_c \text{ on } \Sigma_{B,T} := (\partial\Omega_B - \partial\Omega_H) \times (0, T).
\end{aligned} \tag{4.1}$$

For numerical simulations we rewrite (4.2) in terms of v, u_e and u_s as the strongly coupled parabolic-elliptic PDE-ODE system (see for e.g. [27])

$$\begin{aligned}
\beta c_{\mathrm{m}} \partial_t v + \nabla \cdot \big(\mathbf{M}_{\mathrm{e}}(x) \nabla u_{\mathrm{e}}\big) + \beta I_{\mathrm{ion}}(v, w) = I_e, \qquad & (x,t) \in \Omega_{H,T}, \\
\nabla \cdot \big((\mathbf{M}_{\mathrm{i}}(x) + \mathbf{M}_{\mathrm{e}}(x)) \nabla u_{\mathrm{e}}\big) + \nabla \cdot \big(\mathbf{M}_{\mathrm{i}}(x) \nabla v\big) = I_e - I_i, \qquad & (x,t) \in \Omega_{H,T}, \\
\partial_t w - H(v, w) = 0, \qquad & (x,t) \in \Omega_{H,T}, \\
-\nabla \cdot \big(\mathbf{M}_{\mathrm{s}}(x) \nabla u_{\mathrm{s}}\big) = 0, \qquad & (x,t) \in \Omega_{B,T}.
\end{aligned} \tag{4.2}$$

Now we let $\mathcal{T}_H$ and $\mathcal{T}_B$ (with $\mathcal{T} = \mathcal{T}_H \cap \mathcal{T}_B$) regular partitions of Ω_H and Ω_B, respectively, into tetrahedra K with boundary ∂K and diameter h_K. We define the mesh parameter $h = \max_{K \in \mathcal{T}}\{h_K\}$ and the associated finite element spaces $\boldsymbol{\mathcal{V}}_h$ for the approximation of electrical potentials. For the electrical potentials and ionic variables, we use piecewise linear elements. That is, the involved space is defined as

$$\boldsymbol{\mathcal{V}}_h = \{v \in H^1(\Omega) \cap C^0(\bar{\Omega}) : v|_K \in \mathbb{P}_1(K) \text{ for all } K \in \mathcal{T}\},$$

where $\mathbb{P}_1(K)$ is the set of continuous piecewise linear functions on K. A semidiscrete Galerkin finite element formulation then reads: For $t > 0$, find $\mathbf{u}_h \in \boldsymbol{\mathcal{V}}_h$, $u_e(t), v(t), w(t) \in M_h$, $p \in Q_h$ such that

$$\begin{aligned}
&\beta c_{\mathrm{m}}(\frac{v_h^{n+1}-v_h^n}{\Delta t}, \varphi_{1,h})_{\mathcal{T}_H} - \Big(\mathbf{M}_e(x)\nabla u_{e,h}^{n+1}(t), \nabla\varphi_h\Big)_{\mathcal{T}_H} = (I_{e,h}^{n+1} - \beta I_{\mathrm{ion}}(v_h^{n+1}(t), w_h^{n+1}(t)), \varphi_{1,h})_{\mathcal{T}_H},\\
&\Big((\mathbf{M}_i(x)+\mathbf{M}_e(x))\nabla u_{e,h}^{n+1}(t), \nabla\varphi_{2,h}\Big)_{\mathcal{T}_H} + \Big(\mathbf{M}_i(x)\nabla v_h^{n+1}(t), \nabla\varphi_{2,h}\Big)_{\mathcal{T}_H} = (I_{e,h}^{n+1} - I_{i,h}^{n+1}, \varphi_{2,h})_{\mathcal{T}_H},\\
&(\frac{v_h^{n+1}-v_h^n}{\Delta t}, \phi_h)_{\mathcal{T}_H} = (H(v_h^{n+1}(t), w_h^{n+1}(t)), \phi_h)_{\mathcal{T}_H},
\end{aligned} \tag{4.3}$$

with $\int_{\mathcal{T}_H} u_{e,h}^{n+1} = 0$, $u_{e,h}^{n+1} = u_{s,h}^{n+1}$ on $\partial\mathcal{T}_H$ and

$$\Big(\mathbf{M}_s(x)\nabla u_{s,h}(t)\nabla\varphi_{s,h}\Big)_{\mathcal{T}_B} = 0, \tag{4.4}$$

for all $\varphi_{j,h}, \phi_h \in \boldsymbol{\mathcal{V}}_h$ for $j = 1, 2, s$. Herein, Δt is a fixed time step, the variables with the superscript n are computed at time $t^n = n\Delta t$.

Note that when solving the Bidomain system, the unknowns of the discrete problem are represented by the vector $(v_h, u_{e,h}, u_{s,h}, w_h)$. Moreover the system (4.3) is equivalent to the ODE's:

$$\mathcal{A}\frac{\mathbf{u}_h^{n+1}-\mathbf{u}_h^n}{\Delta t} + \mathcal{B}\mathbf{u}_h^{n+1} = \mathbf{f}_h^n,$$

where $\mathcal{A}$ and $\mathcal{B}$ are the mass and the stiffness matrices, $\mathbf{f}_h^n$ is the source term and $\mathbf{u}_h^n = (v_h, u_{e,h}, u_{s,h}, w_h)$. In the next subsection we give the control and the minimization procedures to our inverse problem.

4.2. **The minimization procedure.** The optimization stage at the discrete level is carried out using the well known nonlinear conjugate gradient method (see e.g. [14]). Here we consider the "discretize-then-optimize" approach, and at each iteration of the minimization procedure, the method requires the solution of the discrete state and adjoint equations. The discrete state equations can be solved by marching forward in time starting from the initial conditions (2.5), while the discrete adjoint equations can be solved by marching backward in time starting from the terminal conditions (3.4).

To compute the optimal control, we improve the initial guess $I_s^0 = I_i^0 - I_e^0$ by using the Jacobian of the reduced objective $\hat{J}^k$ in the conjugate direction $d^k = -\nabla\hat{J}^k$, the latter being also updated at each iteration step, according to the rule $d^{k+1} = -\nabla\hat{J}^k + \varrho^k d^k$, where the sequence $\{\varrho^k\}_k$, is computed using the Hestenes-Stiefel formula [15]

$$\varrho^k = \frac{\big(\nabla\hat{J}^{k+1}, \nabla\hat{J}^{k+1} - \nabla\hat{J}^k\big)_{L^2}}{\big(d^{k-1}, \nabla\hat{J}^{k+1} - \nabla\hat{J}^k\big)_{L^2}}. \tag{4.5}$$

The scaling for the updating of the control at step k is given by δ^k, which is updated following Armijo's rule, i.e., it is reduced by the half until the first Wolfe condition

$$\hat{J}(I_s^k + \delta^k d^k) \le \hat{J}^k + \alpha d^k \nabla\hat{J}^k$$

is satisfied.

Before presenting our numerical examples, we provide a formal description of the overall solution algorithm.

Algorithm 1 (Overall solution algorithm)**.**

(1) *Initialization of parameters.*
 (a) *Choose tolerance α_{abs}, α_{rel}, set $k = 0$, δ^0 and ϱ^0.*
 (b) *Provide an initial guess I_s^0 for the control variable I_s.*
(2) **do** $k = 1, \dots, max\_outer\_iterations$
 (a) **do** $t = t^1, \dots, t^{total\_time\_steps}$
  Solve the state equations (4.2) for (v, u_e, u_i, u_s, w).
 enddo
 (b) *Evaluate the reduced cost functional $\hat{J}^k$.*

(c) **do** $t = t^{total\_time\_steps}, \ldots, t^1$

Being known the state variables (v, u_e, u_i, u_s, w), *compute the solution* (p, p_i, p_e, p_s, q) *of the adjoint problem* (3.3).

enddo

(d) *Compute the Jacobian* $\nabla \hat{J}^k$.

if *the relative and absolute stopping criteria* ($\|\nabla \hat{J}^k\|_{L^2} \leq \alpha_{rel} \|\nabla \hat{J}^0\|_{L^2}$ *and* $\|\nabla \hat{J}^k\|_{L^2} \leq \alpha_{abs}$) *are fulfilled,*

then *exit.*

else

(i) *Compute step length* $\delta^k > 0$.

(ii) *Update the value of the control variable* $I_s^{k+1} = I_s^k + \delta^k d^k$.

(iii) *Compute the step* ϱ^k *from* (4.5).

(iv) *Update the conjugate direction* $d^{k+1} = -\nabla \hat{J}^k + \varrho^k d^k$.

endif

enddo

5. Numerical results

This section is devoted to the presentation of numerical tests to validate the algorithm introduced in the previous section. The state and adjoint equations are discretized using a backward and forward Euler schemes in time, respectively. That is, at each iteration of the gradient algorithm, we sequentially solve the state problem by marching forward in time, whereas the adjoint problem is solved by marching backwards in time starting from terminal conditions.

5.1. **Experiment 1.**

In this first test, we start with the original potential distribution generated for the membrane potential in Figure 1 and the extracellular potential in Figure 2 by using the bidomain as a model for electrical activity of the heart. In these figures, the basal plane is at the bottom, and the apex is at the top, the main axis of the heart is inverted for visualization purposes. In this experiment an applied current (one stimulus) was inserted in a node over the left ventricle at the basal plane during $t < 1$ms. The order of the images is from left to right, top to bottom. From the extracellular potential and the transfer matrix created from the volume conductor model in the equation $Tu_h = u_c$ (herein, T is the transfer operator corresponding to connection between the nodal values over the thorax and the heart), and the relationship from equation the boundary condition (2.4), $u_e = u_s$ on the heart, we create the voltage distribution over the thorax in a forward solution. Using the the minimization of the cost functional J from equation (3.1), for a given regularization value, and the voltage distribution over the thorax we make the reconstruction of the membrane potential over the heart (Figure 3), and the extracellular potential (Figure 4). Employing the operator from the equation $Tu_s = u_c$, we made the reconstruction of the extracellular potential using minimum energy regularization (see Figure 5):

$$\min_{u_e}(||Tu_e - u_c||^2 + \mu||C(u_e - u_e')||^2), \ \mu > 0, \tag{5.1}$$

where C is a constraint matrix, and $u_e' = 0$.

5.2. **Experiment 2.**

In the second test we use the same process as in experiment 1. We apply stimulus at three points instead of one on the basal plane of the heart. The generated electrical activity for the membrane potential and extracelular potential can be seen at Figures 6, and 7 respectively. Using the minimization of the functional J (equation (3.1)) we make the reconstruction of both extracellular and membrane potential for the thorax distribution generated using a three-point stimulus, in Figures 8 and 9, respectively. Utilizing the minimum energy minimization from equation 5.1, we make the reconstruction of the extracellular potential (Figure 10).

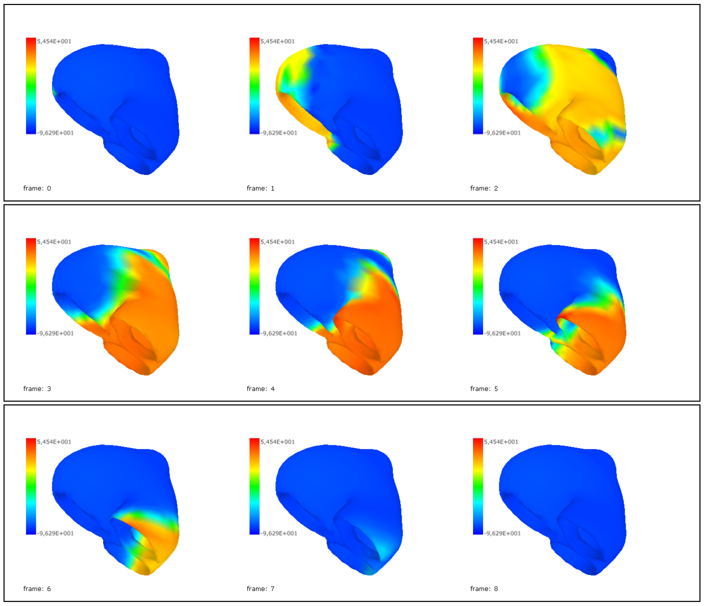

FIGURE 1. Membrane Potential for the heart at t=0 ms, 50 ms, 100 ms, 150 ms, 200 ms, 250 ms, 300 ms, 350 ms, and 400 ms for one applied impulse at the left ventricle.

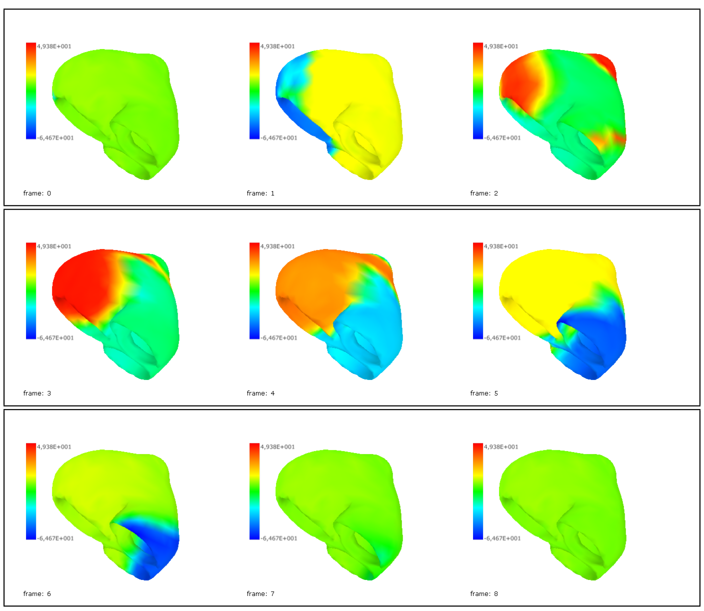

FIGURE 2. Extracellular Potential for the heart at t=0 ms, 50 ms, 100 ms, 150 ms, 200 ms, 250 ms, 300 ms, 350 ms, and 400 ms for one applied impulse at the left ventricle.

5.3. **Experiment 3.** Using the data sets generated by the forward problem in Figure 1, we add 1% noise to the potential distribution at the thorax. Then, we make the reconstruction of membrane and extracellular potential. To create the noise we did the following; first we calculate the range from the dataset values over the thorax Range=Max-Min. Then for each value

$$\mathrm{Data}_{i,j} = \mathrm{Data}_{i,j} + 0.01 * \mathrm{Range} * \mathrm{Random}, \qquad \mathrm{Random} = -1, \dots, 1. \tag{5.2}$$

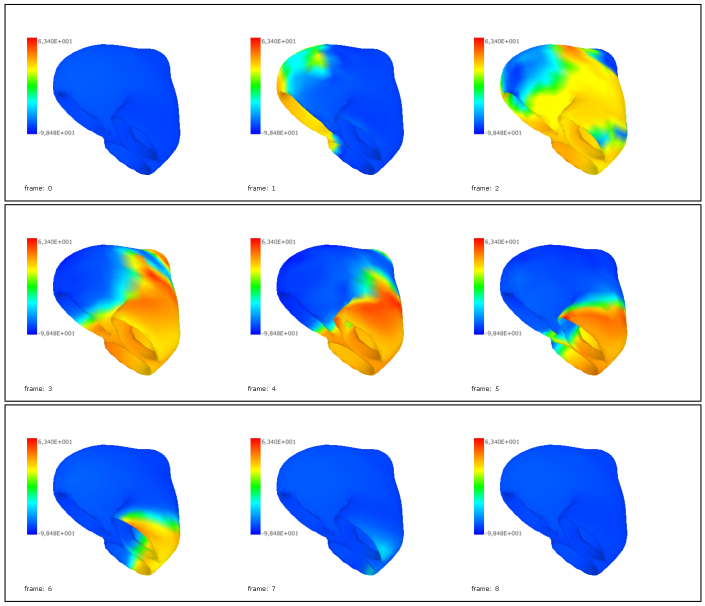

FIGURE 3. Membrane Potential reconstructed by using the bidomain operator for the heart at t=0 ms, 50 ms, 100 ms, 150 ms, 200 ms, 250 ms, 300 ms, 350 ms, and 400 ms.

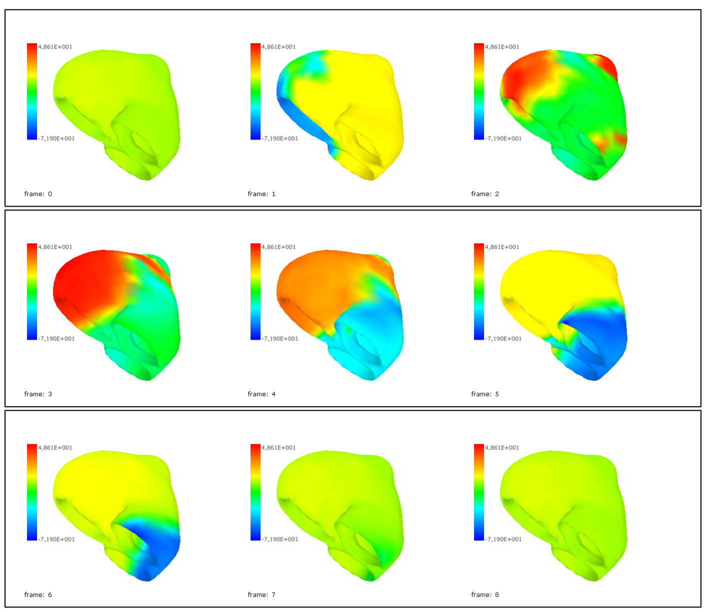

FIGURE 4. Extracellular Potential reconstructed with the bidomain operator for the heart at t=0 ms, 50 ms, 100 ms, 150 ms, 200 ms, 250 ms, 300 ms, 350 ms, and 400 ms.

As in Experiment 1, we make the reconstruction of the membrane potential, extracellular potential, and extracellular potential by minimum energy potential, Figures 11, 12, and 13 respectively from the potential distribution over the thorax with added noise.

5.4. **Experiment 4.** For the membrane potential distribution Figure 1, we calculate the forward solution in the thorax using a non-homogeneous operator transfer matrix (including the lungs). Then, for the inverse

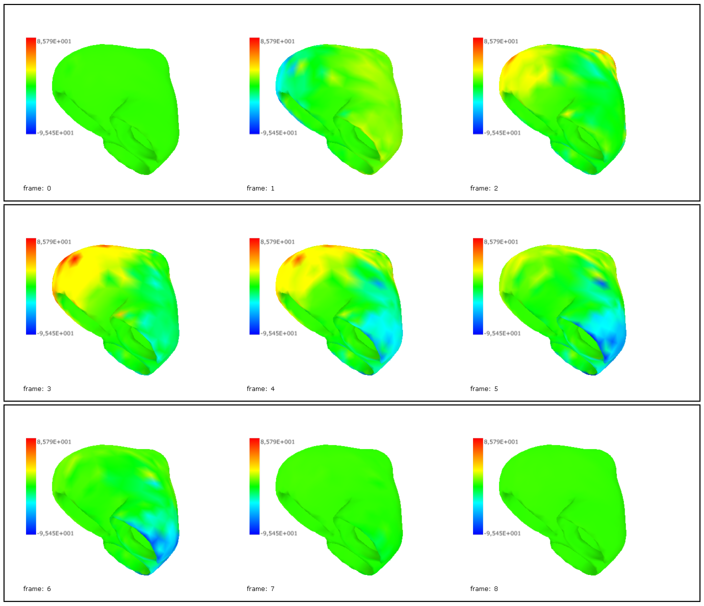

Figure 5. Extracellular Potential reconstructed with the minimum energy norm for the heart at t=0 ms, 50 ms, 100 ms, 150 ms, 200 ms, 250 ms, 300 ms, 350 ms, and 400 ms.

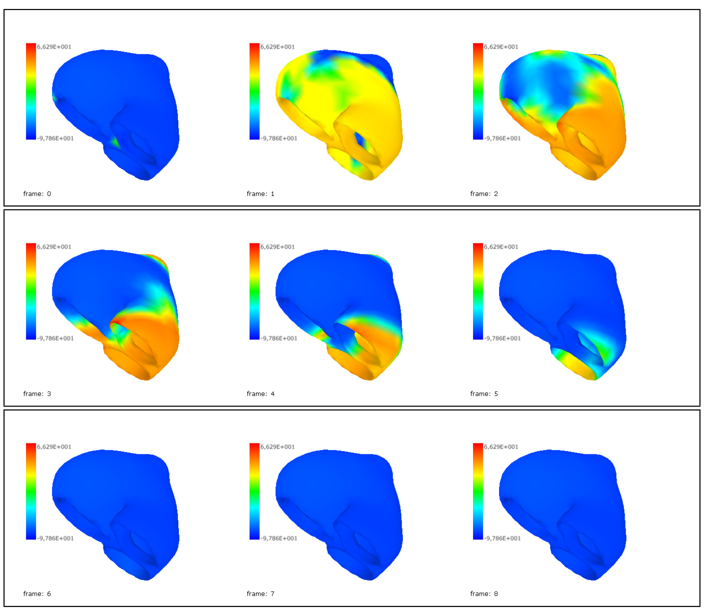

Figure 6. Membrane Potential for the heart at t=0 ms, 50 ms, 100 ms, 150 ms, 200 ms, 250 ms, 300 ms, 350 ms, and 400 ms for three applied stimulus at the basal plane on the heart.

solution we use the generated distribution at the thorax, and solve the inverse problem with an homogeneous operator. The procedure is detailed in Figure 14. The reconstructed membrane, and extracellular potential distribution are in Figures 15, 16 and 17 using the bidomain operator. The reconstruction using the procedure of the minimum energy is in Figure 17.

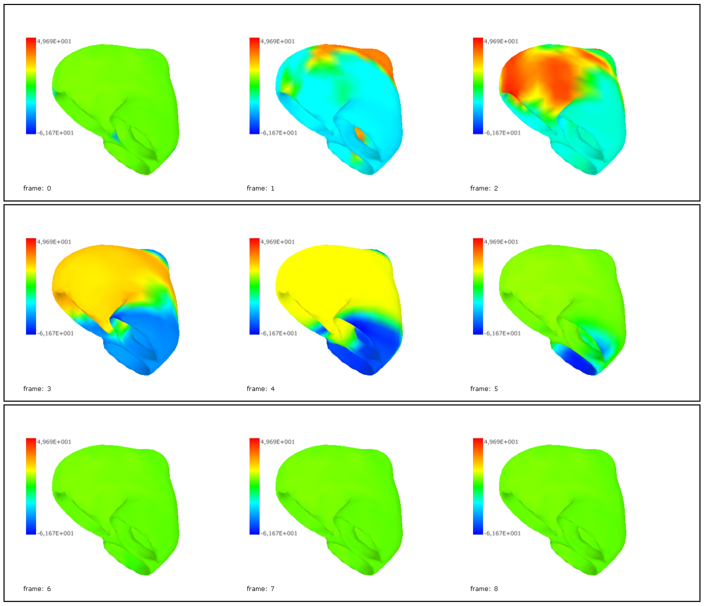

FIGURE 7. Extracellular Potential for the heart at t=0 ms, 50 ms, 100 ms, 150 ms, 200 ms, 250 ms, 300 ms, 350 ms, and 400 ms for three applied stimulus at the basal plane on the heart.

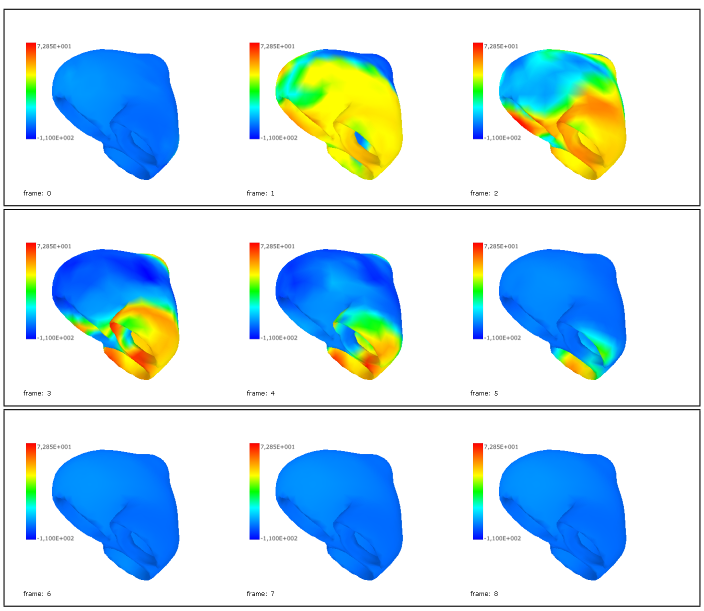

FIGURE 8. Membrane Potential reconstructed by using the bidomain operator for the heart at t=0 ms, 50 ms, 100 ms, 150 ms, 200 ms, 250 ms, 300 ms, 350 ms, and 400 ms for the three point stimulus.

5.4.1. *Summary of Results.* For each of the tests the error was calculated with the following formula:

$$error = \frac{\sum(u_{h_i} - u_{c_i})^2}{\sum(u_{h_i})^2} \tag{5.3}$$

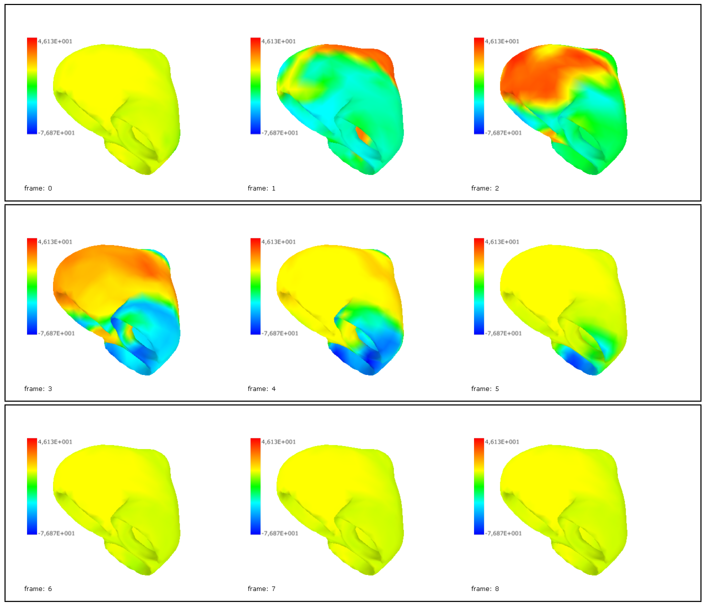

FIGURE 9. Extracellular Potential reconstructed with the bidomain operator for the heart at t=0 ms, 50 ms, 100 ms, 150 ms, 200 ms, 250 ms, 300 ms, 350 ms, and 400 ms for the three point stimulus.

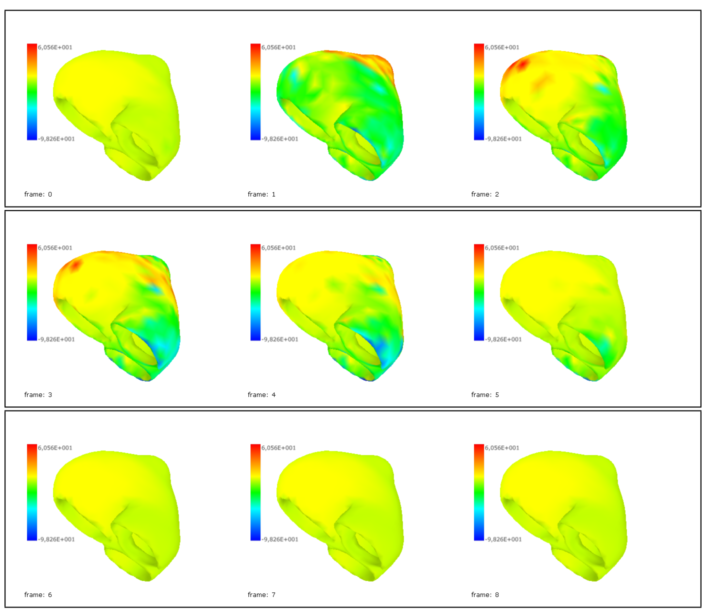

FIGURE 10. Extracellular Potential reconstructed with the minimum energy norm for the heart at t=0 ms, 50 ms, 100 ms, 150 ms, 200 ms, 250 ms, 300 ms, 350 ms, and 400 ms for the three point stimulus.

for the difference between the original distribution and the calculated: using the bidomain inverse operator, and the static regularization using the minimum energy norm. The time simulated is 1 second.

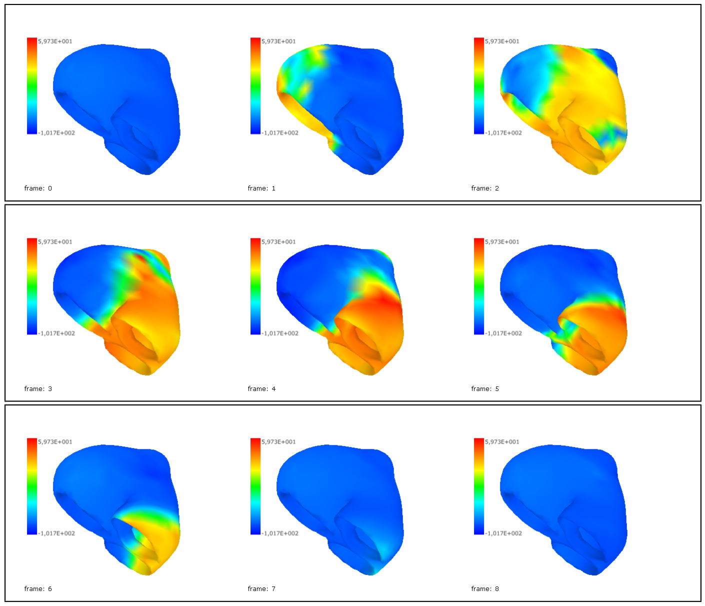

FIGURE 11. Membrane Potential reconstructed by using the bidomain operator for the heart at t=0 ms, 50 ms, 100 ms, 150 ms, 200 ms, 250 ms, 300 ms, 350 ms, and 400 ms for the 1 point stimulus, with a 1% noise over the thorax' measures.

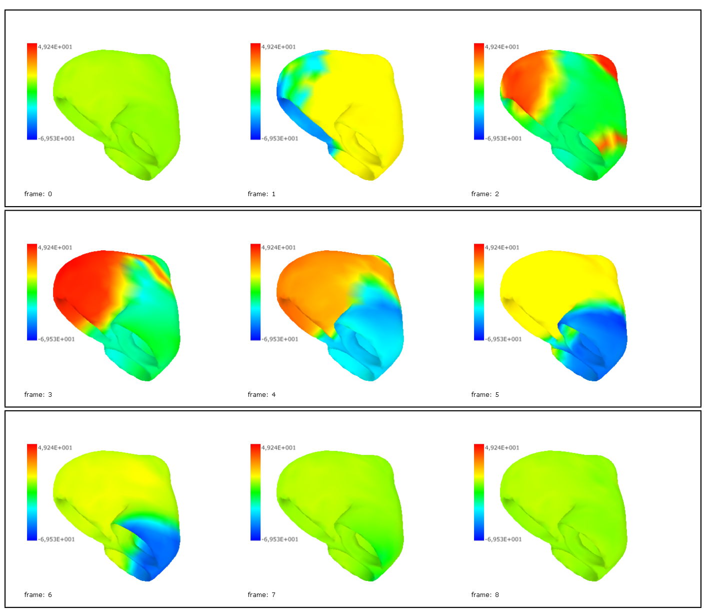

FIGURE 12. Extracellular Potential reconstructed by using the bidomain operator for the heart at t=0 ms, 50 ms, 100 ms, 150 ms, 200 ms, 250 ms, 300 ms, 350 ms, and 400 ms for the 1 point stimulus, with a 1% noise over the thorax' measures.

	Test1	Test2	1% Noise	Homogeneous-Non Homogeneous
$MinimumExtracellular$	0.6564	0.6947	0.9664	0.8106
$bidomainExtracellular$	0.0790	0.2318	0.0841	0.3375
$bidomainMembrane$	0.0091	0.0219	0.0097	0.0386

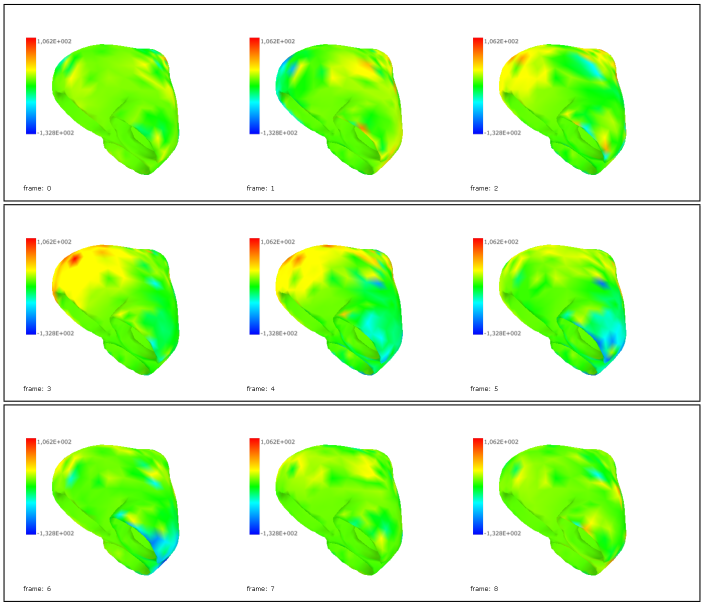

FIGURE 13. Extracellular Potential reconstructed with the minimum energy norm for the heart at t=0 ms, 50 ms, 100 ms, 150 ms, 200 ms, 250 ms, 300 ms, 350 ms, and 400 ms from the three point stimulus at the thorax.

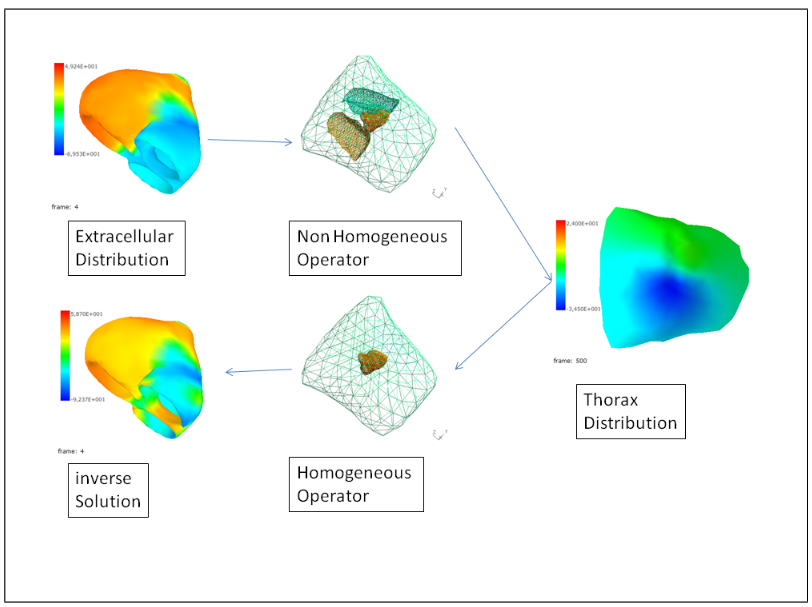

FIGURE 14. Procedure of the experiment.

6. CONCLUSION

In our study, we aimed at improving noninvasive reconstructions of the electrical cardiac sources from body surface potential measurements (BSPMs), considering the torso as a volume conductor. It is fascinating that the heart dynamic model (bidomain model) improves quality of reconstruction of the electrical cardiac surface. Following the series of experiments were presented our study, our results are promising. Note that

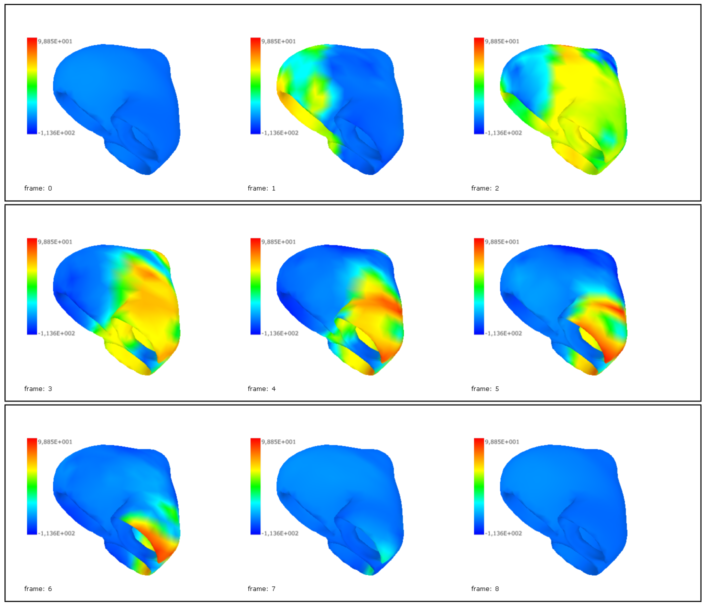

FIGURE 15. Membrane Potential reconstructed by using the bidomain operator for the heart at t=0 ms, 50 ms, 100 ms, 150 ms, 200 ms, 250 ms, 300 ms, 350 ms, and 400 ms for the 1 point stimulus, with a homogeneous operator for a non-homogeneous created body surface potentials.

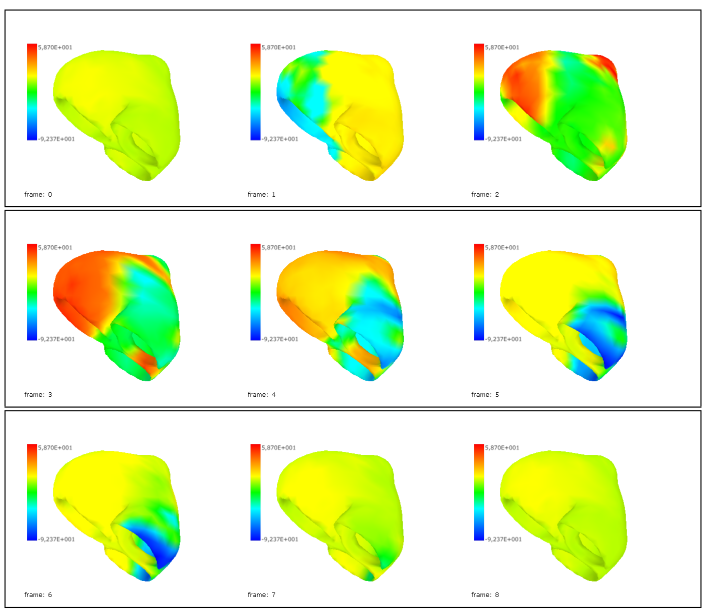

FIGURE 16. Extracellular Potential reconstructed by using the bidomain operator for the heart at t=0 ms, 50 ms, 100 ms, 150 ms, 200 ms, 250 ms, 300 ms, 350 ms, and 400 ms for the 1 point stimulus, with a homogeneous operator for a non-homogeneous created body surface potentials.

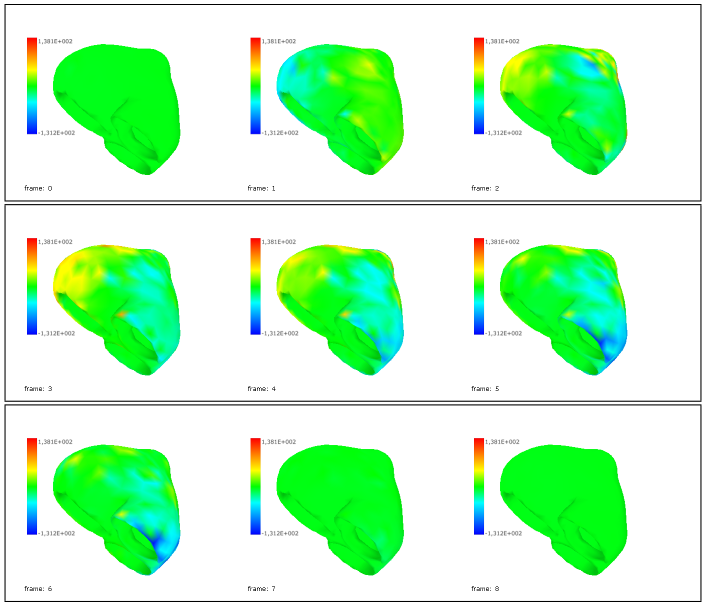

Figure 17. Extracellular potential calculated by using the minimum energy solution for the heart at t=0 ms, 50 ms, 100 ms, 150 ms, 200 ms, 250 ms, 300 ms, 350 ms, and 400 ms for the 1 point stimulus, with a homogeneous operator for a non-homogeneous created body surface potentials.

the heart dynamic model cannot be neglected in the inverse problem of electrocardiology. Our reconstructions using the bidomains equations are considerably better than those obtained with quasi-static heart model. Moreover, comparing to quasistatic inverse ECG, there is a significant difference if we use non-homogeneous operator transfer matrix and we solve the inverse problem with an homogeneous operator. Finally we want to mention that our method described in this paper may be useful clinically for detecting and localising cardiac arrythmias and ischemia.

References

[1] M. Bendahmane, R. Bürger, R. Ruiz, A finite volume scheme for cardiac propagation in media with isotropic conductivities, Mathematics and Computers in Simulation, (2010), (80):1821-1840.

[2] M. Bendahmane, R. Bürger, R. Ruiz, K. Schneider, Adaptive multiresolution schemes with local time stepping for two-dimensional degenerate reaction-diffusion systems, Appl. Numer. Math. (2009), (59)7, 1668–1692.

[3] M. Bendahmane, K.H. Karlsen, Analysis of a class of degenerate reaction-diffusion systems and the bidomain model of cardiac tissue, Netw. Heterog. Media 1 (2006) 185–218.

[4] M. Bendahmane, K.H. Karlsen, Finite volume methods for degenerate reaction-diffusion systems modeling the Cardiac electric field, Applied Numerical Mathematics (2009), (59)9, 2266-2284.

[5] E. Cherry, H. Greenside, C.S. Henriquez, Efficient simulation of three–dimensional anisotropic cardiac tissue using an adaptive mesh refinement method, Chaos 13 (2003) 853–865.

[6] P. Colli Franzone, P. Deuflhard, B. Erdmann, J. Lang, L.F. Pavarino, Adaptivity in space and time for reaction–diffusion systems in electro-cardiology, SIAM J. Sci. Comput. 28 (2006) 942–962.

[7] P. Colli Franzone, L.F. Pavarino, A parallel solver for reaction-diffusion systems in computational electro-cardiology, Math. Models Meth. Appl. Sci. 14 (2004) 883–911.

[8] P. Colli Franzone, L.F. Pavarino, B. Taccardi, Simulating patterns of excitation, repolarization and action potential duration with cardiac Bidomain and Monodomain models, Math. Biosci., 197 (2005), 35–66.

[9] P. Colli Franzone, G. Savaré, Degenerate evolution systems modeling the cardiac electric field at micro- and macroscopic level, in: A. Lorenzi, B. Ruf (Eds.), Evolution equations, semigroups and functional analysis, Birkhäuser, Basel, 2002, pp. 49–78.

[10] E. Entcheva, J. Eason, F. Claydon, R. Malkin, Spatial effects from bipolar current injection in 3D myocardium: implications for conductivity measurements, Computers in Cardiology 7 (1997) 717–720.

[11] R. FitzHugh, Impulses and physiological states in theoretical models of nerve membrane, Biophys. J. 1 (1961) 445–465.
[12] R.M. Gulrajani, The forward and inverse problems of electrocardiography, Engineering in Medicine and Biology Magazine, IEEE, (17)5 (1998) 84–101.
[13] S. Guofa, X. Ling and J. Mingfeng, Solving the Electrocardiography Inverse Problem by Using an Optimal Algorithm Based on the Total Least Squares Theory, Natural Computation, (5) 2007 115–119. ICNC 2007.
[14] W.W. Hager, H. Zhang, A survey of nonlinear conjugate gradient methods, Pacific J. Optim. 2 (2006) 35–58.
[15] M.R. Hestenes, E.L. Stiefel, Methods of conjugate gradients for solving linear systems, J. Research Nat. Bur. Standards, 49 (1952) 409–436.
[16] A.L. Hodgkin, A.F. Huxley, A quantitative description of membrane current and its application to conduction and excitation in nerve, J. Physiol. 117 (1952) 500–544.
[17] J. Keener, J. Sneyd, Mathematical Physiology, Corr. Second Printing, Springer-Verlag, New York, 2001.
[18] O. A. Ladyzenskaja, V. A. Solonnikov, and N. N. Uralceva. Linear and quasilinear equations of parabolic type. American Mathematical Society, Providence, R.I., 1967.
[19] C. Mitchell, D. Schaeffer, A two-current model for the dynamic of cardiac membrane, Bull. Math. Biol. 65 (2001) 767–793.
[20] J.S. Nagumo, S. Arimoto, S. Yoshizawa, An active pulse transmission line simulating nerve axon, Proc. Inst. Radio Eng. 50 (1962) 2061–2071.
[21] D. Noble, A modification of the Hodgkin-Huxley equations applicable to Purkinje fibre action and pacemaker potentials, J. Physiol. 160 (1962) 317–352.
[22] M. Pennacchio, V. Simoncini, Efficient algebraic solution of reaction-diffusion systems for the cardiac excitation process, J. Comp. App. Math. 145-1 (2002) 49–70.
[23] W. Quan, S. Evans, H. Hastings, Efficient integration of a realistic two-dimensional cardiac tissue model by domain decomposition, IEEE Trans. Biomed. Eng. 45 (1998) 372–385.
[24] H. Saleheen, K. Ng, A new three–dimensional finite-difference bidomain formulation for inhomogeneous anisotropic cardiac tissues, IEEE Trans. Biomes. Eng. 45 (1998) 15–25.
[25] K. Skouibine, N. Trayanova, P. Moore, A numerically efficient model for simulation of defibrillation in an active bidomain sheet of myocardium, Math. Biosci. 166 (2000) 85–100.
[26] J. Simon, Compact sets in the space Lp(0, T;B), Ann. Mat. Pura Appl., (4) 146 (1987) 6596.
[27] J. Sundnes, G.T. Lines, X. Cai, B.F. Nielsen, K.-A. Mardal, A. Tveito, Computing the Electrical Activity in the Heart, Springer-Verlag, Berlin, 2006.
[28] J. Trangenstein, C. Kim, Operator splitting and adaptive mesh refinement for the Luo-Rudy I model, J. Comput. Phys. 196 (2004) 645–679.
[29] L. Tung, A Bi-Domain Model for Describing Ischemic Myocordial D-C Currents, PhD thesis, MIT, Cambridge, MA, 1978.
[30] D. Wang, R. Kirby and C. Johnson, C, Resolution Strategies for the Finite-Element-Based Solution of the ECG Inverse Problem, Biomedical Engineering, IEEE Transactions, (57)2 (2010) 220–237.
[31] Y. Yamashita, Theoretical Studies on the Inverse Problem in Electrocardiography and the Uniqueness of the Solution Biomedical Engineering, IEEE Transactions, (29)11 (1982) 719–725.
[32] W.-J. Ying, A Multilevel Adaptive Approach for Computational Cardiology, PhD Thesis, Department of Mathematics, Duke University, 2005.
[33] W.-J. Ying, D.J. Rose, C.S. Henriquez, Efficient fully implicit time integration methods for modeling cardiac dynamics, Technical Report, Duke University, 2007.